QUARTERLY JOURNAL OF THE ROYAL METEOROLOGICAL SOCIETY
Q. J. R. Meteorol. Soc. **133**: 1629–1641 (2007)
Published online in Wiley InterScience
(www.interscience.wiley.com) DOI: 10.1002/qj.105

RMetS
ROYAL METEOROLOGICAL SOCIETY

Variance scaling in shallow-cumulus-topped mixed layers

R. A. J. Neggers,* B. Stevens and J. D. Neelin
Department of Atmospheric and Oceanic Sciences, University of California, Los Angeles

ABSTRACT: Scaling of thermodynamic variance in shallow-cumulus-topped mixed layers is studied using large-eddy simulation (LES). First, the performance of the top-down scaling (the turbulent flux at mixed-layer top divided by w_*) is evaluated for transient shallow-cumulus convection over land. The results indicate that this scaling fails to capture all the variance in the top half of the mixed layer when shallow cumulus clouds are present. A variance-budget analysis is then performed, to derive a new scaling for the variance at mixed-layer top, which differs from the standard top-down scaling by a factor of one Richardson number. The essential new features of the proposed scaling are that the local vertical gradient is retained and that a balance is assumed between gradient production of variance and removal by transport and dissipation, using an adjustment time-scale given by w_*/h. Evaluation against LES for a range of different cases, including a dry convective boundary layer as well as steady-state marine and transient continental shallow cumulus, reveals a data-collapse of the newly-scaled variance, for all hours and all cases in the top half of the mixed layer. The corresponding vertical structure is shown to resemble a power-law function. The results suggest that the structure of variance in the dry convective boundary layer is similar to that in the sub-cloud mixed layer. In transient situations, the scaling reproduces the time-development of variance at sub-cloud mixed-layer top. The new cloud-base variance scale is then further interpreted in the context of statistical cloud schemes, which depend on the variance as the second moment of the associated probability density function. The results suggest that the area fraction of the moist convective thermals uniquely depends on the ratio of cloud-base transition-layer depth to sub-cloud mixed-layer depth. This puts 'valve'- or ventilation-type closures for the cloud-base mass flux in the context of the variance budget for the sub-cloud layer. Copyright © 2007 Royal Meteorological Society

KEY WORDS shallow cumulus; variance scaling; transition layer; mass-flux closure

Received 2 September 2006; Revised 6 February 2007; Accepted 9 February 2007

1. Introduction

The parametrization of vertical transport of heat, humidity and momentum by shallow-cumulus-cloud populations has been the subject of intensive research (see, for example, (Arakawa, 2004) for a recent review). The mass-flux approach, wherein the vertical advective transport by organized updraughts is explicitly modelled, has emerged as one of the more successful methods (e.g. Ooyama, 1971; Yanai *et al*., 1973; Betts, 1975; Siebesma and Cuijpers, 1995). The mass flux is defined as the product of air density, convective area fraction, and vertical velocity of the associated updraughts. While most bulk-closure methods parametrize the mass flux as a single entity, the area fraction and vertical velocity can also be modelled individually. For instance, the updraught vertical velocity can be estimated from the integrated mixed-layer buoyancy flux (e.g. Grant, 2001), while the associated convective area fraction can be retained and explicitly parametrized (e.g. Bretherton *et al*., 2004; Neggers *et al*., 2004). The area fraction can be estimated using an assumption for the underlying probability density function (PDF) of the thermodynamic state variables (Sommeria and Deardorff, 1977), as constrained by the prediction of one or more of its moments. Even the simplest of these PDF-based approaches requires knowledge of the variance of temperature and humidity. This raises the question motivating this study: what determines the structure of the variance at the top of the sub-cloud mixed layer?

Standard similarity theory for the convective mixed layer, or mixed-layer scaling, grew out of attempts to understand the similarity structure of the surface layer in the early 1970s (see, for example, (Stull, 1988) for a review). Near the surface in shear-free convective layers it is often argued that conserved scalars follow the free-convective temperature scaling of (Wyngaard *et al*., 1971; Kaimal *et al*., 1976), in which the dimensionless variance of some scalar c scales as

$$\frac{{\sigma_c}^2}{c_*^2} = \alpha \left(\frac{z}{h}\right)^{-\frac{2}{3}}, \tag{1}$$

where

$$c_* \equiv \frac{\overline{w'c'}_0}{w_*}.$$

* Correspondence to: R. A. J. Neggers, Royal Netherlands Meteorological Institute (KNMI) PO Box 201, 3730 AE De Bilt, The Netherlands.
E-mail: Roel.Neggers@knmi.nl

The overline denotes the mean value, and the prime denotes fluctuations, so that $c = \overline{c} + c'$. Values at $z = 0$ are denoted by subscript 0; values at the top of the sub-cloud mixed layer, $z = h$, will be denoted by subscript h. The Deardorff, or convective, velocity scale is denoted by w_*.

Field measurements from Minnesota reported by Kaimal *et al.* (1976) show that the potential-temperature variance conforms well to Equation (1) in the lower part of the mixed layer ($z < 0.1h$) with the constant of proportionality $\alpha = 1.8$. However, this scaling works less well for $z > 0.1h$. Between $0.1h$ and $0.5h$, θ^2 tends to decrease more rapidly than the theory predicts, and θ^2 tends to increase again above $0.5h$. Kaimal *et al.* (1976) recognized the tendency of θ^2 to increase with z above $0.5h$ as a signature of entrainment: a process not accounted for in the arguments leading up to Equation (1). Subsequent work by a number of investigators (e.g. Deardorff, 1974b; Nicholls and LeMone, 1980; Lenschow *et al.*, 1980; Caughey, 1982) reinforced these findings, and helped motivate the concepts of top-down and bottom-up scalar diffusion (Wyngaard and Brost, 1984). According to these ideas, the fundamental asymmetry of the convective forcing of the convective boundary layer (CBL), whereby the buoyancy flux is positive at the surface and some negative fraction of the surface forcing at the top of the CBL, causes scalars mixing into the CBL from the top (top down) to diffuse through the CBL differently from scalar fluxes originating at the bottom (bottom up).

Using these ideas, and noting that any scalar c can be written as a linear combination of its top-down and bottom-up components c_t and c_b, Moeng and Wyngaard (1984) showed that the scalar variance through the depth of the dry CBL can be well represented by superimposing the scalar variance expected for pure top-down and bottom-up scalars:

$$\sigma_c^2 = c_{h*}^2 f_h\left(\frac{z}{h}\right) + 2c_{h*}c_{s*}f_{hs}\left(\frac{z}{h}\right) + c_{s*}^2 f_s\left(\frac{z}{h}\right). \quad (2)$$

In this expression, the quantities

$$\left.\begin{aligned} c_{h*} &= \overline{w'c'}_h/w_* \\ c_{s*} &= \overline{w'c'}_0/w_* \end{aligned}\right\}, \quad (3)$$

are separate scalings measuring the relative contributions of the top-down and bottom-up components of the scalar, with $\overline{w'c'}_0$ and $\overline{w'c'}_h$ denoting the turbulent flux at the surface and top of the planetary boundary layer (PBL) respectively. The height variations of the component variances are carried by the functions f_h and f_s, which Moeng and Wyngaard (1984) deduced empirically on the basis of existing field data and large-eddy simulation (LES).

We ask how well Equation (2) captures the variance profiles of liquid-water potential temperature θ_l and total specific humidity q_t, in the sub-cloud layers of boundary layers topped by shallow cumulus. To answer this question, we use a suite of simulations drawn from past studies, ranging from nearly-stationary maritime shallow cumulus to highly non-stationary cases of shallow cumulus over land. The non-stationary cases are all tied to the diurnal cycle, and allow us to explore several different convective regimes within one simulation. This significantly broadens the parameter space, compared to studies of more stationary conditions.

Figure 1 shows hourly variance profiles, obtained from LES, of the diurnal variation of a fair-weather cumulus case over land (see Section 2 for its description). The variance profiles are normalized by the mixed-layer-top scale c_{h*}^2, as defined in Equation (3). Near $z = h$ (defined as the height of minimum buoyancy flux), this scale dominates the contributions from the f_s and f_{hs} terms in Equation (2). In other words, use of the height-dependent scaling given by Equation (3) would not improve the scaling in the upper part of the mixed layer. Although c_{h*}^2 explains more of the variance than does c_{s*}^2, the normalized variance profiles still exhibit considerable spread. This is especially evident during the later hours of the diurnal cycle, when convection is more intense: the top scaling c_{h*}^2 then underestimates the variance. The figure also illustrates a limitation of Equation (2), in that f_h, which Moeng and Wyngaard (1984) set to $14(1 - z/h)^{-2/3}$ for $z > 0.9h$, has a singularity at $z = h$, thus further hinting at the inappropriateness of Equation (2) as z approaches h.

These observations motivate further study of the vertical structure of variance in shallow-cumulus-topped mixed layers. In this paper, a new top-down variance scaling is presented, which differs from that of Equation (3) by its incorporation of the local gradient. It is found that this scaling better reproduces the structure, magnitude and time-development of mixed-layer variance, for both stationary and transient shallow-cumulus cases and a transient case of dry convection. The new cloud-base-variance scaling is then further interpreted in the context of statistical cloud schemes, by assuming the form of the PDFs of humidity and temperature. The

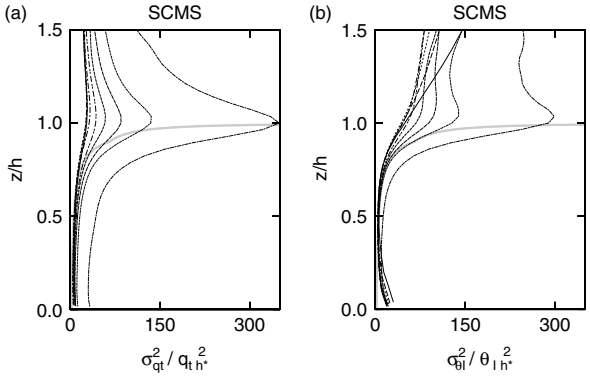

Figure 1. Scaled hourly-mean vertical profiles of the variance of (a) total specific humidity q_t, and (b) liquid-water potential temperature θ_l, during the continental cumulus case based on the Small Cumulus Microphysics Study (SCMS). The height is scaled by the mixed-layer height h, defined as the height of minimum buoyancy flux, and the variance is normalized by the mixed-layer-top scale c_{h*}^2, as defined in Equation (3). The grey lines indicate the f_h structure function.

DOI: 10.1002/qj

results suggest that the area fraction of the moist convective thermals uniquely depends on the ratio of cloud-base transition-layer depth to sub-cloud mixed-layer depth. This places the type of mass-flux closures that explicitly parametrize this area fraction – also known as 'valve'-type closures (e.g. Mapes, 2000; Bretherton *et al*., 2004; Neggers *et al*., 2004) – in the context of the full variance budget.

In Section 2, the LES model, as well as the cases that form the basis of this study, will be described. In Section 3, the new scaling will be presented; in Section 4 it is evaluated against the LES. In Section 5 the important role of the cloud-base transition layer in the new scaling will be explored, implying a new closure formulation for the mass-flux area fraction. The implications of the results are discussed in Section 6, and some concluding remarks are given in Section 7.

2. LES model and case descriptions

The LES is performed using the model of the Royal Netherlands Meteorological Institute (KNMI), as described in detail by Cuijpers and Duynkerke (1993). The results presented in this paper are based on a reanalysis of a suite of simulations established over time, of which many were performed in order to take part in the LES intercomparison studies organized by the boundary-layer working group of the Global Energy and Water Experiment Cloud System Study (GCSS) (Browning, 1993). The details of the model and the numerical simulations, including the domain size and resolution, differ between cumulus cases, as described below.

Four shallow-cumulus cases are simulated. Two of these represent relatively steady marine conditions, while the other two represent more transient continental conditions. The first marine case is based on a period of undisturbed trade-wind convection capped by a weak inversion, as synthesized from observations made during the Barbados Oceanic and Meteorological Experiment (BOMEX) (Holland and Rasmusson, 1973; Nitta and Esbensen, 1974). Further details are given by Siebesma *et al*. (2003). The second marine case is similar, although capped by a much stronger inversion, below which the cumulus clouds detrain into a shallow stratocumulus layer. It is based on a synthesis of observations taken during an undisturbed period of the Atlantic Trade-Wind Experiment (Augstein *et al*., 1973, 1974). Further details are given by Stevens *et al*. (2001).

The first continental diurnal-cycle case is based on measurements taken at the Central Facility of the Southern Great Plain site of the Atmospheric Radiation Measurement (ARM) programme (Stokes and Schwartz, 1994). The shallow-cumulus cloud layer was observed to slowly deepen after onset. The set-up of the LES case is described by Brown *et al*. (2002). The second continental cumulus case is based on the Small Cumulus Microphysics Study (SCMS) (Knight and Miller, 1998; French *et al*., 1999; Laird *et al*., 2000). Some relevant boundary-layer measurements, and the set-up of the LES case, are described by Neggers *et al*. (2003). Although similar to the ARM case, it is somewhat more humid, and features a relatively high cloud cover in the LES, with a peak value of about 40% shortly after cloud onset. The cloud layer also deepens relatively rapidly compared to the ARM case.

The dry CBL case is roughly based on a previous intercomparison case of LES codes for the dry CBL (Nieuwstadt *et al*., 1993). Several modifications are introduced in order to increase transience: prescribed surface fluxes of $\overline{w'\theta'} = 100$ Wm^{-2} and $\overline{w'q'} = 200$ Wm^{-2}, a prescribed radiative-cooling tendency of -1 K day^{-1}, and an initial state consisting of a 700 m-deep mixed layer with $\overline{q} = 8$ g kg^{-1} and $\overline{\theta} = 300$ K, topped by a layer with lapse rates of $\Gamma_q = -1.67$ g kg^{-1} km^{-1} and $\Gamma_\theta = 2$ K km^{-1}. In the first 4 h of simulation, the inversion rises from 0.7 km to 1.8 km.

3. Variance-budget analysis

The failure of c_{h*} to scale the variance correctly as z approaches h could reflect differences in the scaling of the dry convective layer as compared to the sub-cloud layer, but more probably reflects the inappropriateness of the formulation near the top of the dry convective layer. We argue that a successful scaling should reflect the coupling between the dry convective (sub-cloud) layer and the (cloud) layer above, and therefore should incorporate information from both layers, as well as the local stability of the interface (transition) layer separating them (e.g. Augstein *et al*., 1974; Albrecht *et al*., 1979; Yin and Albrecht, 2000). In revisiting this issue, we return to the full prognostic equation for the thermodynamic variance. Following Deardorff (1974a), the variance budget can be written as

$$\frac{\partial \sigma_c^2}{\partial t} = -2\overline{w'c'}\frac{\partial \overline{c}}{\partial z} - \frac{\partial \overline{w'c'c'}}{\partial z} - \epsilon. \qquad (4)$$

Here $\overline{w'c'c'}$ is the turbulent flux of variance, and ϵ is the molecular dissipation of variance. We have assumed horizontal homogeneity because it is enforced in LES and it simplifies the analysis.

We focus on the variance budget at the mixed-layer top, because the variances at this height are critical to a determination of cloud fraction. Using LES of a developing clear CBL, Deardorff (1974b) showed that at the top of the dry CBL the gradient-production term is the only source term, representing dry mixed-layer thermals that overshoot into the strong gradient and generate variance accordingly. Production is countered by transport and dissipation. Figure 2 illustrates that this structure is similar in shallow-cumulus situations. To the extent that h is the only relevant length scale in the problem, one expects the variance dissipation to decay on a large-eddy time-scale (Nieuwstadt and Brost, 1986):

$$\tau \equiv \frac{h}{w_*}. \qquad (5)$$

DOI: 10.1002/qj

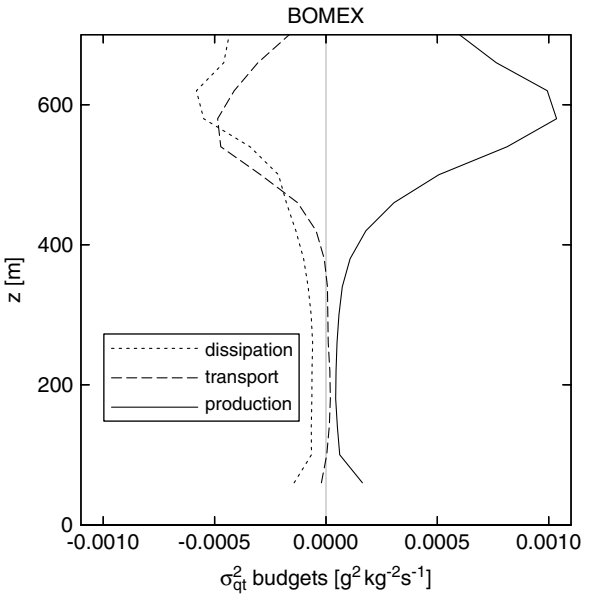

Figure 2. The steady-state humidity-variance-budget equation (4) for the BOMEX case, as sampled in LES. Production and transport are calculated, and dissipation is obtained as their residual. Cloud base in BOMEX is at about 600 m.

Because in the balance all the leading-order terms must follow the same scaling, the steady-state variance budget of Equation (4) then becomes:

$$-\overline{w'c'}_h \frac{\partial \overline{c}}{\partial z}\Big|_h \propto \frac{\sigma_c^2\Big|_h}{\tau}, \tag{6}$$

where the subscript h refers to the local value at mixed-layer top. Support for these arguments is provided by Grant and Lock (2004), who show that mixed-layer scaling of turbulent kinetic energy still holds in the transition zone. A further justification is provided in Appendix A, where we approach the scaling from the perspective of the transport term: in this framework, transport and dissipation act together to reduce any variance that is produced and maintained by mixed-layer thermals overshooting into the transition layer. Relation (6) suggests a new local scaling $c_\#$ for the variance at mixed-layer top:

$$c_\#^2 \equiv -\overline{w'c'}_h \frac{\partial \overline{c}}{\partial z}\Big|_h \frac{h}{w_*}. \tag{7}$$

The remainder of this paper explores this scaling in more depth.

In previous scaling of shallow-cumulus variance (Grant and Brown, 1999; Lenderink and Siebesma, 2000), the time-scale of relaxation of variance has been modelled as the ratio of cloud-layer depth to a vertical-velocity scale that is a function of the convective available potential energy (CAPE) of the cloud layer. This choice may be appropriate in the cloud layer, but becomes problematic in the mixed layer in cases of forced cumulus convection (cumulus humilis), in which the clouds never reach their level of free convection and the velocity scale associated with CAPE is zero or negative. A good example is the period shortly after cloud onset in the transient continental convection. A further feature of Equation (7) is that it is only applied *locally* at mixed-layer top. As a result, through the vertical gradient $\partial\overline{c}/\partial z$, the small jump in temperature and humidity that is often observed at shallow-cumulus cloud base (e.g. Augstein *et al*., 1974; Albrecht *et al*., 1979; Yin and Albrecht, 2000) is incorporated into the scaling.

4. LES results

The new variance scaling (7) is now evaluated using LES. Figures 3 and 4 show hourly-averaged variance profiles normalized by $c_\#$ for all the PBL cases described in Section 2, irrespective of the presence of clouds. The scaling applies best in the height range $0.6 < z/h \leq 1$, corresponding to heights where the production of variance at the top of the PBL might be expected to exert more influence than, say, near-surface variance production.

These results suggest that a typical vertical structure exists in the scaled variance profile in the top half of the mixed layer. To illustrate this, the scaled variance profiles of all hours and all cases are plotted together in Figure 5. Because f_h behaves poorly near $z = h$, we fit a new power-law function to the scaling region. To this end, the same data are plotted on logarithmic axes: see Figure 6. Here a linear relation with slope b implies that the variance depends on the dimensionless height ratio raised to the power of b (so-called 'similarity of the second kind'):

$$\frac{\sigma_c^2}{c_\#^2} = 0.9\left(\frac{z}{h}\right)^{b_\mathrm{c}}, \tag{8}$$

where the exponents for specific humidity $b_\mathrm{q} = 4$ and potential temperature $b_\theta = 6$ are different. Both fits are also shown in Figure 5. We believe that differences in the exponent reflect the different ways in which humidity and temperature project onto buoyancy, but this warrants further investigation. The variance peaks at the level of maximum gradient, which is slightly higher than the level of minimum buoyancy flux, as already observed by Deardorff (1974b) for the dry CBL. This is reflected in the constants of proportionality used in Equation (8), which are slightly less than one. Close to the surface, the new variance scaling fails, because cloud-base characteristics become less relevant at levels further away from it. At these levels one expects the surface scalings to dominate. This motivates combining the surface and mixed-layer-top scalings into one relation (e.g. Moeng and Wyngaard, 1984):

$$\sigma_c^2(z) = 1.8\left(\frac{z}{h}\right)^{-\frac{2}{3}} c_{s*}^2 + 0.9\left(\frac{z}{h}\right)^{b_\mathrm{c}} c_\#^2. \tag{9}$$

Figure 7 shows the time series of the variances at mixed-layer top for three of the cases. The performance

DOI: 10.1002/qj

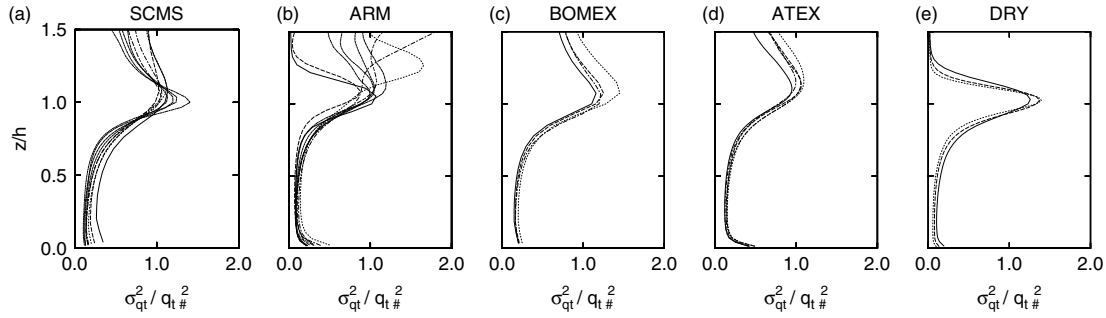

Figure 3. Vertical profiles of the moisture variance, as in Figure 1(a), but for all cases and with the variance normalized by the new scaling $c_\#^2$. The height is scaled by the mixed-layer depth h.

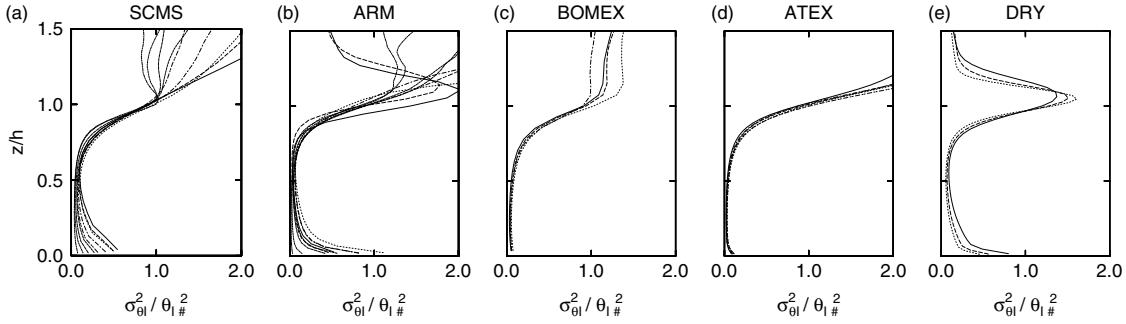

Figure 4. As Figure 3, but for the scaled liquid-water potential-temperature variance.

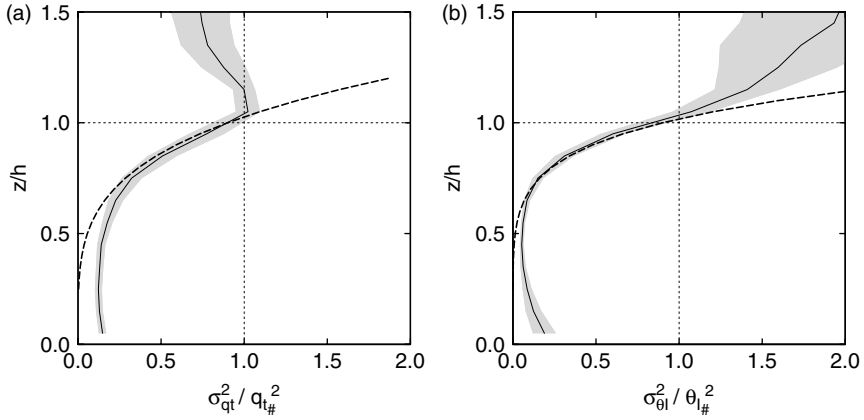

Figure 5. Scaled variance profiles for (a) moisture and (b) liquid-water potential temperature, as in Figures 3 and 4, but averaged over all cases and all hours. The black solid line is the mean, while the grey area indicates the standard deviation. The thick dashed line represents the power-law fit (Equation (8)).

of $c_\#$ is compared to that of the surface scaling c_{s*} and top-down scaling c_{h*}. The new variance scaling $c_\#$ is most successful in reproducing the time evolution as seen in LES. The surface scaling c_{s*} tends to reach its maximum at a much earlier time than the scalings for mixed-layer top. Using c_{h*} correctly shifts the maximum towards later times, but is still not sufficient. Both the scalings that fail to capture information on the local vertical gradient also fail to capture the variance minimum that occurs in the ARM case at hour 7.

Figure 8 shows the time series of the local vertical gradients of humidity and temperature at mixed-layer top for the two cumulus-over-land cases. In the course of the day, these gradients change significantly. In general, the mixed-layer top experiences destabilization in the first hours and stabilization in the last hours of the diurnal cycle. This reflects the development of the coupling between the mixed layer and the cloud layer. In this respect, the ARM and SCMS cases develop quite differently during the first hours, the ARM case being much more stable above the mixed layer. During the 7th hour in the ARM case, the mixed-layer top suddenly destabilizes; this is accompanied by a more rapid deepening of the cloud layer (see Figure 9(b)). This

DOI: 10.1002/qj

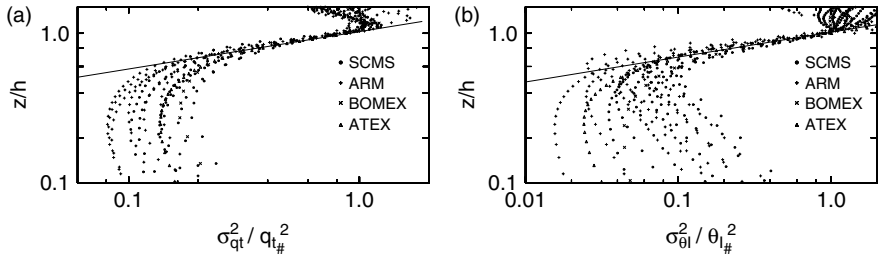

Figure 6. Logarithmic scatter plot of the scaled variance profiles of all cases and all hours. The black solid line represents a power-law fit through the upper part of the sub-cloud layer, which shows evidence of scaling behaviour. The slope of the fit corresponds to the exponent, which is 4 for specific humidity and 6 for potential temperature (see Equation (8)).

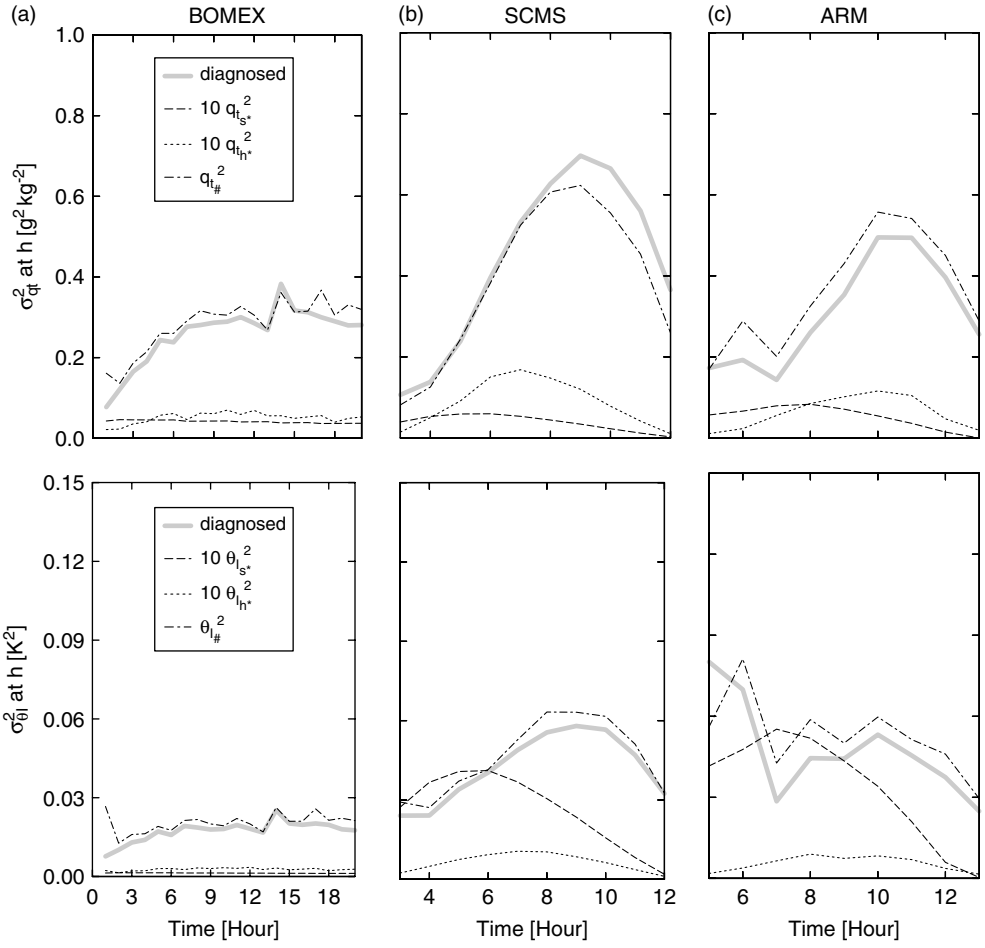

Figure 7. Time series of the diagnosed variances of q_t and θ_l at mixed-layer top (grey), and the corresponding variance scales c_{s*}, c_{h*} and $c_\#$ (black), during (a) BOMEX, (b) SCMS, and (c) ARM. Some scales are multiplied by a factor of 10 for purposes of comparison.

sudden weakening of the gradients is accompanied by a significant decrease in variance (see Figure 7(c)). This further suggests that the variance near h is coupled to the vertical gradients at h, and that scalings that incorporate the local gradients can be expected to behave with more fidelity.

5. Mass-flux area fraction

The results illustrate that the structure of the cloud-base transition layer significantly affects the local variance. This interface layer is now studied in more detail, with the aim of parametrizing those of its properties that appear in the new variance scaling (7). This is necessary for the broad class of models that do not provide this information naturally, and it may give more insight into the important role of the cloud-base transition layer in shallow-cumulus convection.

Figure 9 shows the typical vertical structure of a shallow-cumulus-topped boundary layer. The cloud base height z_b is defined as the height of maximum cloud-core fraction, which is defined as the area fraction of

DOI: 10.1002/qj

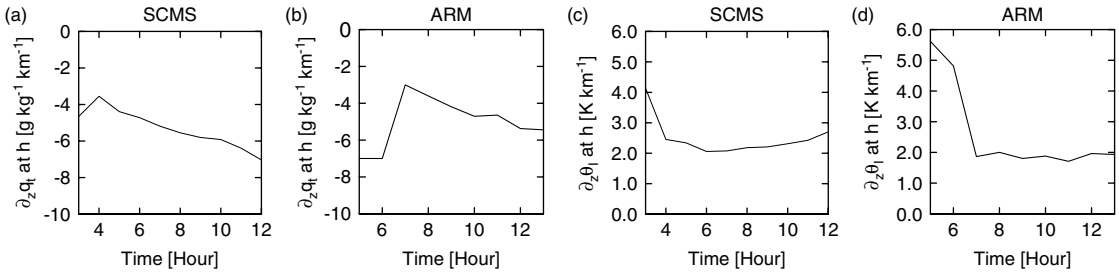

Figure 8. Time series of the local vertical gradients of total specific humidity and liquid-water potential temperature at mixed-layer top h, during the SCMS and ARM cases.

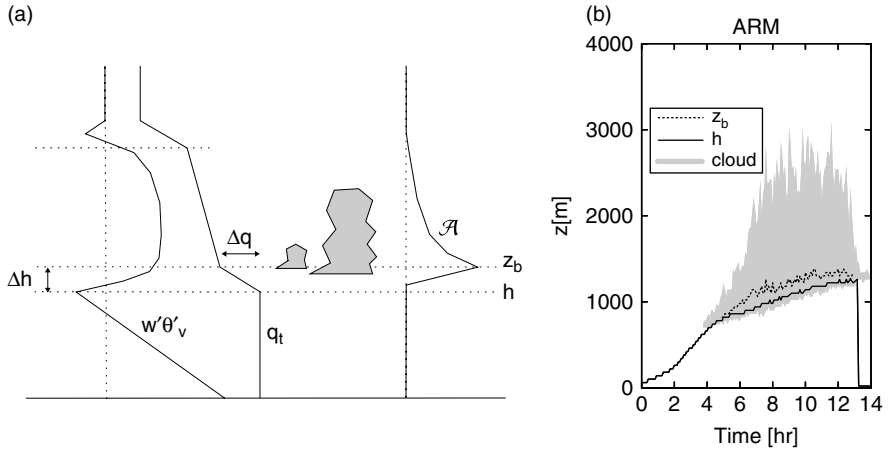

Figure 9. Typical structure of the shallow-cumulus-topped mixed layer. (a) Profiles of the buoyancy flux $\overline{w'\theta'_v}$, total specific humidity, and cloud-core fraction $\mathcal{A}$ (the symbols are defined in the text). (b) Time series of h and z_b for the ARM case. The cloud layer is shaded (grey). The transition layer is situated between h and z_b.

positively-buoyant clouds (also called the 'moist convective thermals'). In prototype shallow-cumulus convection, the cloud core does most of the vertical transport (Siebesma and Cuijpers, 1995): this justifies its use in the bulk-mass-flux approach. Following (Grant, 2001), we define the transition layer as the layer of depth Δh between h and z_b. Lenderink and Siebesma (2000) were the first to apply the mass-flux approach in the variance-production term. Combined with a bulk-gradient approach over the transition-layer depth, this gives for Equation (7):

$$c_\#^2 = M\frac{\Delta c^2}{\Delta h}\frac{h}{w_*}, \tag{10}$$

where M is the cloud-base mass flux and Δc is the jump in the mean vertical profile $\overline{c}$ over the transition layer. Here the humidity excess of the moist convective thermals over the dry environment has been assumed to be proportional to Δc. Figure 10(a) shows that this assumption is supported by LES. This proportionality is due to the moist convective thermals still carrying properties of the mixed layer where they originate. Their collective volumetric mass flux M is defined as the product of their area fraction $\mathcal{A}$ and their vertical velocity, which at cloud base scales well with w_* (Neggers *et al.*, 2004).

$$M = \mathcal{A}\omega_* \tag{11}$$

This eliminates w_* in Equation (10), yielding:

$$c_\#^2 \approx \mathcal{A}\Delta c^2\frac{h}{\Delta h}. \tag{12}$$

Thus, retaining the convective area fraction in the mass flux (e.g. Neggers *et al.*, 2004; Neggers *et al.*, 2006) makes it appear in the cloud-base variance scaling. This is intriguing from the perspective of statistical parametrization of area fractions (Sommeria and Deardorff, 1977), which itself depends on the variance as the second moment of the turbulent distribution of humidity and temperature. As a consequence, there are two equations for the two unknowns $\mathcal{A}$ and σ_c, so that $\mathcal{A}$ and σ_c are defined implicitly. In other words, scaling σ_c with $c_\#$ would yield a parametrization for $\mathcal{A}$.

This implicit representation of $\mathcal{A}$ still requires the definition of the shape function of the associated turbulent distribution. One could use a normal distribution (e.g. Sommeria and Deardorff, 1977; Bougeault, 1982). However, such a distribution would have global support, and it is perhaps more appropriate in this problem to use a distribution with compact support. For example, the most extreme q_t value at cloud base that can theoretically occur – that of an undiluted updraught – can never exceed its value at its starting height in the mixed layer. We choose to explore these issues using the beta distribution (e.g. Tompkins, 2002), whose density is expressed

DOI: 10.1002/qj

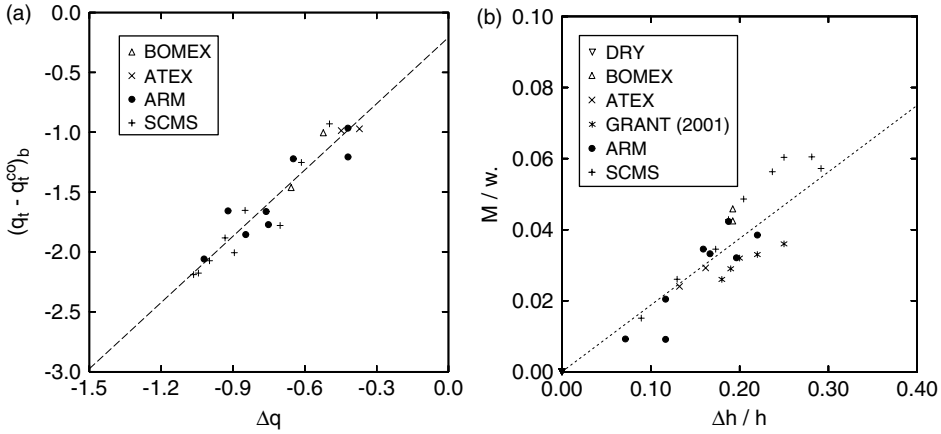

Figure 10. (a) Difference between mean-state total specific humidity $\overline{q_t}$ and that of the cloud core q_t^{co} at z_b, plotted against the jump in total specific humidity $\overline{q_t}$ between mixed-layer top h and cloud base z_b. The points represent hourly averages from all cases. The dashed line represents the least-squares linear fit. (b) Scatter plot of $\Delta h/h$ against M/w_*. The points represent hourly averages from all cases. The results of (Grant, 2001) are also included. The dotted line represents the least-squares fit of Equation (17), giving $p = 2.2$.

by the beta function:

$$B(p, r) = \int_0^1 x^{p-1}(1-x)^{r-1}\mathrm{d}x, \tag{13}$$

where p and r are the shape parameters of the distribution. The standard deviation of the beta distribution is related to the distribution boundaries a and b:

$$\sigma \equiv \frac{b-a}{p+r}\sqrt{\frac{pr}{p+r+1}}. \tag{14}$$

Figure 11 supports a choice for the boundaries satisfying:

$$b - a = 2\Delta c. \tag{15}$$

Assuming a non-skewed distribution ($p = r$), Equation (14) then gives

$$\frac{\sigma_c^2}{\Delta c^2} = \frac{1}{2p+1}. \tag{16}$$

Thus the variance is related to the local jump in $\overline{c}$ through the shape function of the associated PDF. Substituting this ratio into the cloud-base variance scaling (12) finally gives

$$\mathcal{A} = \frac{\Delta h}{h}\frac{1}{2p+1}. \tag{17}$$

This relation states that the area fraction of the cloudy, buoyant thermals is uniquely determined by the ratio of transition-layer depth to sub-cloud mixed-layer depth, multiplied by a term dependent on the shape of the distribution.

Equation (17) is verified by comparing the ratio M/w_* at z_b to the depth ratio $\Delta h/h$ for all cumulus cases: see Figure 10(b). Despite some scatter, the existence of a relation between $\mathcal{A}$ and $\Delta h/h$ is supported by the LES results (cf. (Grant, 2001), where this ratio is assumed constant). The apparent linearity of the LES data suggests that p is constant, implying that the shape of the PDF at cloud base is more or less case-independent. Fitting relation (17) to the LES data gives

$$p \approx 2.2. \tag{18}$$

The side panels in Figure 11 illustrate that this beta distribution resembles the LES distributions reasonably well. Some of the scatter in Figure 10(b) can be attributed to the low vertical resolution of these LES runs, which at 40 m was of the same order of magnitude as Δh. This causes deviations in $\Delta h/h$ of up to 40 m /800 m = 0.05 (taking a typical value for h). Additional simulations at higher vertical resolution, and using a shorter averaging time-scale, could help clarify this issue.

In the derivation of Equation (17), the numerator Δc of the local vertical gradient has dropped out against σ_c, but the denominator Δh is preserved, introducing a coupling between the area fraction of the moist convective thermals and the depth of the transition layer. For example, in situations of high transition-layer stability (large gradients, or small Δh), $\mathcal{A}$ is small, corresponding to a reduced mass flux. The transition layer thus acts as a 'valve' in cumulus transport. On the other hand, through the dissipation time-scale, the mixed-layer depth has entered the equation. As a result, deepening sub-cloud mixed layers imply decreasing convective area fractions: a characteristic feature of diurnal cycles of shallow cumulus, which is indeed often observed in nature and in LES (e.g. Brown *et al.*, 2002; Neggers *et al.*, 2004).

6. Discussion

6.1. Comparison to (Moeng and Wyngaard, 1984)

We now return to the (Moeng and Wyngaard, 1984) scaling c_{h*}, as discussed in Section 1, and ask why and how the new variance scaling $c_\#$ is different. Comparing

DOI: 10.1002/qj

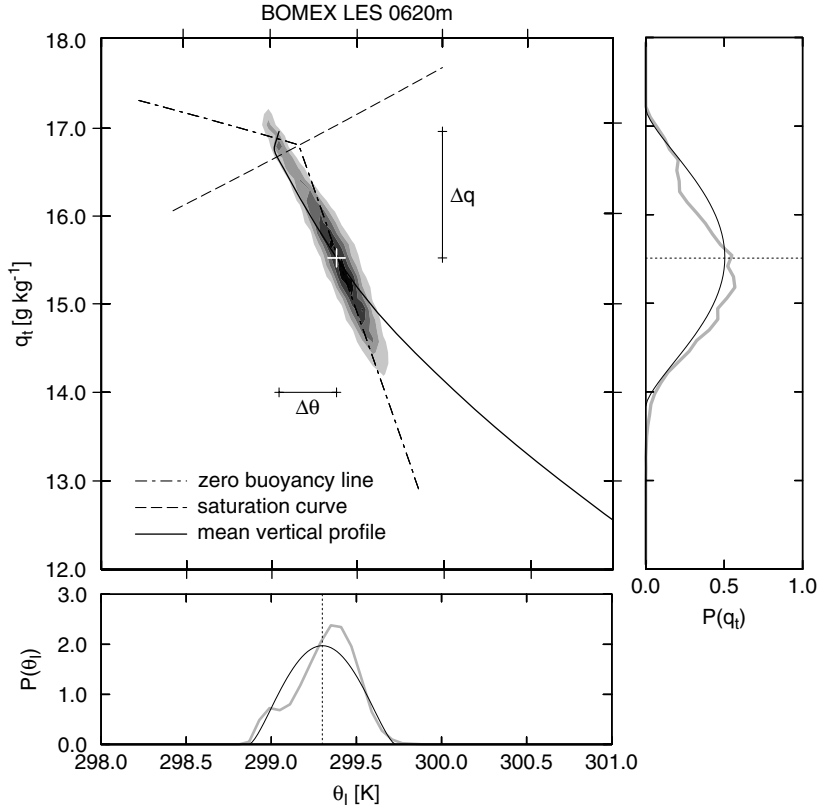

Figure 11. Joint PDF of q_t and θ_l at BOMEX cloud base ($z_b = 620$ m), as obtained from LES. The complete mean vertical profile is indicated by the solid line; its values at z_b are indicated by the cross. The saturation curve and the zero-buoyancy line at this particular level are also shown. q_{sat} is the point where the joint PDF intersects the saturation curve, and q_{zb} corresponds to its intersection with the moist part of the zero-buoyancy line. The transition-layer jumps Δq and $\Delta\theta_l$ are also shown. The two side panels show the PDF $P(x)$ (grey lines), and the PDF of the beta distribution with $p = r = 2.2$ (black lines).

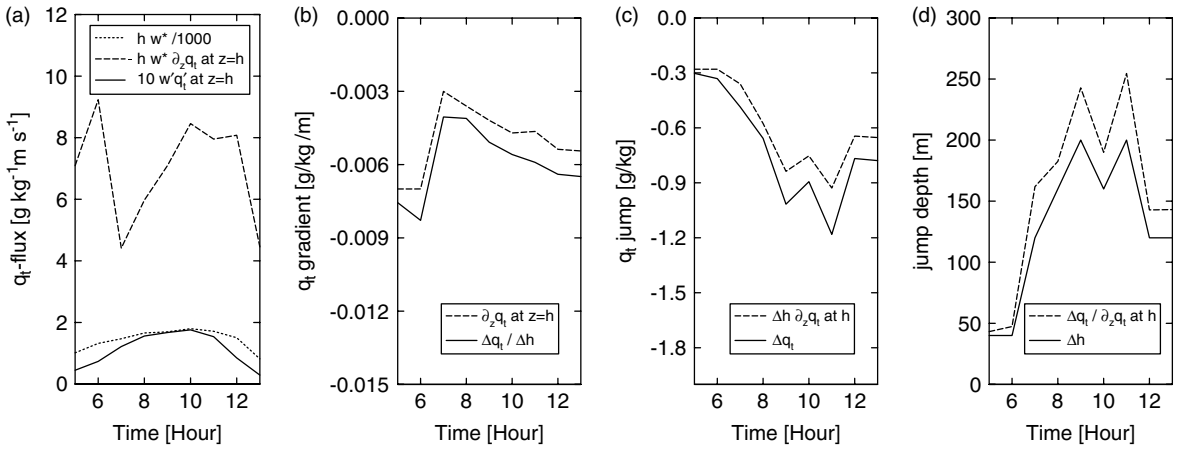

Figure 12. (a) Evaluation of the validity of Equation (19) in LES, for the ARM case. All parameters in the equation are diagnosed individually. Some terms are amplified by a decimal factor, for purpose of display. (b) Comparison of the bulk gradient of q_t over the transition layer to the local gradient at $z = h$. (c) Transition-layer jump of q_t, and (d) transition-layer depth: dashed lines indicate the values obtained using the local gradient at $z = h$.

Equations (3) and (7), we see that the two scales are only the same if

$$\overline{w'c'}_h \approx -hw_* \frac{\partial \overline{c}}{\partial z}\Big|_h. \tag{19}$$

Figure 12(a) shows the two sides of Equation (19), confirming that they are indeed not the same and that the vertical gradient (plotted in Figure 12(b)) is causing the difference in time development between the scales. Further breakup of the gradient in Figure 12(c) and (d) reveals that growth of the transition-layer depth Δh is uniquely responsible for the sudden decrease in the gradient at $t = 7$ h, counteracting a strengthening of the jump Δc in the process.

To further illustrate that c_{h*} and $c_{\#}$ are indeed different theoretically and do not revert to each other in some

DOI: 10.1002/qj

limit, we now apply the bulk-gradient approach over the transition-layer depth (see Figure 12(b)),

$$\left.\frac{\partial \overline{c}}{\partial z}\right|_h \approx \frac{\Delta c}{\Delta h}, \tag{20}$$

and the flux-entrainment relation at h,

$$\overline{w'c'}_h = -E\Delta c = -\frac{A}{Ri_\mathrm{h}} w_* \Delta c, \tag{21}$$

where E is the top-entrainment velocity, A is a constant of proportionality, and

$$Ri_\mathrm{h} \equiv \frac{g\Delta\theta_\mathrm{v} h/\theta_0}{w_*^2} \tag{22}$$

is the standard bulk Richardson number, with $g\Delta\theta_\mathrm{v}/\theta_0$ the buoyancy jump associated with the transition layer. If Equation (19) holds, then substitution of Equations (20) and (21) would imply that

$$\frac{\Delta h}{h} \propto Ri_\mathrm{h}. \tag{23}$$

However, we can prove that Equation (23) cannot hold, by studying the equilibrium mass budget of the sub-cloud mixed layer (Stevens, 2006; Neggers *et al*., 2006). In equilibrium, neglecting large-scale divergence for simplicity (typically $w_\mathrm{LS} \ll E$ in shallow-cumulus conditions), the cumulus mass flux M should equal the top-entrainment rate E. As both share dependence on w_*, one can equate the associated factors of proportionality in E and M. Together with Equation (17), as implied by the variance scaling, this gives:

$$\frac{\Delta h}{h} \propto Ri_\mathrm{h}^{-1}. \tag{24}$$

This gives:

$$\frac{g}{\theta_0}\Delta\theta_\mathrm{v}\Delta h = B w_*^2, \tag{25}$$

where the constant B carries the proportionality in Equation (24). Accordingly, in equilibrium, Δh corresponds to the depth of the layer in which:

- the dry plumes involved in entrainment, and whose energy scales with w_*^2, lose their kinetic energy; and
- cumulus updraughts condense and reach positive buoyancy.

Clearly Equations (23) and (24) cannot both be true, and so Equation (19) cannot hold. Finally, substituting Equation (21) into Equation (3), and Equations (20), (21) and (24) into Equation (7), we see that the new local scaling $c_\#$ is indeed theoretically different from the (Moeng and Wyngaard, 1984) scaling $c_{\mathrm{h}*}$ by a factor of one Richardson number:

$$c_\# \propto Ri_\mathrm{h} c_{\mathrm{h}*}. \tag{26}$$

6.2. Transient convection

Combining Equations (24) and (17) relates the equilibrium area fraction of transporting cumulus updraughts to the interface Richardson number at mixed-layer top:

$$\mathcal{A} = \frac{A}{Ri_\mathrm{h}}. \tag{27}$$

Using typical values of $E = 1$ cm s^{-1} and $w_* = 1$ ms^{-1} (e.g. Stevens, 2006) gives the equilibrium value $\mathcal{A} = 0.01$, explaining the small convective cloud fractions that are characteristic of shallow-cumulus convection. However, what happens when the boundary layer is not in equilibrium? Then E does not necessarily equal M, and $\mathcal{A}$ can deviate from Equation (27). In fact, as illustrated in Figure 10(b), in transient conditions $\mathcal{A}$ (and with it $\Delta h/h$) changes significantly: from the dry convective limit ($\mathcal{A} \to 0$) up to $\mathcal{A} = 0.05$. This suggests that it is crucial to allow Δh to be flexible in order to allow the system to approach equilibrium: during the equilibration process, Δh and h will adjust to values such that M becomes equal to E, as expressed by the equilibrium condition (27).

It is interesting to interpret the role of Δh in the equilibration process in the context of a recent study by Neggers *et al*. (2006). They studied sub-cloud mixed-layer equilibration using a simple bulk model including cumulus mass flux, parametrized statistically as a function of w_* and the normalized saturation deficit at mixed-layer top. They found that the sensitivity to saturation thus introduced in the mass flux through $\mathcal{A}$ constitutes a negative feedback mechanism, which can explain the approach towards the equilibrium state of Equation (27). If $\mathcal{A}$ can be parametrized as a function of $\Delta h/h$, as implied by combining variance scaling with the mass-flux approach, then Δh should play the same equilibrating role, acting as a 'valve' in the cumulus mass flux. Figure 9(b) illustrates that this is indeed the case, showing how Δh opens and closes at the onset and decay, respectively, of the cumulus-cloud layer. This suggests that modelling $\mathcal{A}$ as a function of transition-layer depth provides an alternative way to represent the concept of moist-convective inhibition in PBL schemes (e.g. Mapes, 2000; Bretherton *et al*., 2004).

It is tempting to think of Equation (27) as a *cumulus equilibrium constraint*. However, it should be noted that Ri_h is not an external variable, but is highly dependent on the small internal jump $\Delta\theta_\mathrm{v}$ between the cloud and sub-cloud layers. The eventual equilibrium value of Ri_h is determined by the differential large-scale forcings in the cloud layer and the sub-cloud layer, as well as by the boundary conditions at the bottom and top of the PBL (the surface and the lower troposphere respectively). This topic is explored in more detail by Neggers *et al*. (2006), and also in ongoing work by Bretherton and Park (submitted to JAS, 2006). Understanding what controls Ri_h may thus be important in helping to determine cloud fraction, as well as in applying the $c_\#$ scalings in models with coarse vertical resolution.

DOI: 10.1002/qj

7. Concluding remarks

A new local scaling $c_\#$ for the variance at mixed-layer top is introduced, as defined by Equation (7), with the aim of addressing shortcomings in the standard top-down scaling for the dry CBL in situations where shallow cumulus clouds are present. The novelty of $c_\#$ is that, in addition to the entrainment flux, it incorporates information on local (transition-layer) stability and the convective-mixed-layer turnover time-scale. This significantly improves the scaling of variance in transient cumulus situations. The local vertical gradient changes considerably during the first hours after cloud onset, and affects the local variance through the flux-gradient-production term. The collapse of the data, for a range of different LES cases, supports the generality of the scaling. Indeed, the fact that the scaling also works for dry convective layers not topped by cumulus convection provides yet another demonstration of the similarity between dry convective layers and the sub-cloud layer in the presence of shallow, non-precipitating, convection.

Through the definition of variance as the second moment of a turbulent distribution, the physics in the variance budget is shown to imply a relation between the mass-flux area fraction and the ratio of transition-layer depth to mixed-layer depth. The transition-layer depth is shown to represent the negative feedback mechanism between cloud-base mass flux, local stability and proximity to saturation at mixed-layer top (Bretherton *et al*., 2004; Neggers *et al*., 2006). The mixed-layer depth h in general increases during diurnal cycles, thus reducing $\mathcal{A}$ with time. This inverse relation is consistent with observations in nature and LES (Brown *et al*., 2002; Neggers *et al*., 2004).

The role of the transition layer in shallow-cumulus convection has been studied extensively in the past. The present study shows how variance and transition-layer depth enter the problem. Our results suggest new opportunities for parametrization. For example, the variance scaling could be used in combination with statistical cloud schemes (Neggers *et al*., 2006). Furthermore, parametrizing the transition-layer depth could be an alternative approach to representing the impact of the transition layer: for example, by relating it to the *moist instability depth scale* of model updraughts rising out of the mixed layer. In a forthcoming study ('A dual mass-flux model for boundary-layer convection', in preparation for the *Journal of the Atmospheric Sciences*), these concepts are explored using the PBL scheme of the ECMWF Integrated Forecasting System.

The LES cases used for evaluation in this study are of different natures, featuring a dry CBL case as well as steady-state marine and transient continental cumulus cases, with surface Bowen ratios ranging from about 0.03 to 0.5. Nevertheless, there are still different scenarios for which it is unknown whether the variance scaling applies. For example, it is interesting to study cases with strong vertical wind shear, as mechanical turbulence might represent a significant source in the variance budget. The validity of the variance scaling against observations also remains a topic for future research.

Studying the variance structure in transient shallow-cumulus cases such as ARM and SCMS has the advantage that we gain an understanding of their behaviour for more complex scenarios than steady-state situations. This significantly expands the parameter range that is covered. The time-dependence of the variance introduces challenges for parametrization. The closures as presented here have been directly inspired by the study of these diurnal-cycle cases. This emphasizes the importance of setting up as many different cases as possible, preferably based on reliable observational data. The work of the GCSS boundary-layer working group to extract cases from observations has directly contributed to the wealth of moist-convective cases that are now available to the boundary-layer-modelling community.

Acknowledgements

We thank Chris Bretherton and an anonymous reviewer for their insightful comments on this study. This research was supported in part by National Science Foundation grants DMS-0139666, ATM-0082529 and ATM-0342625, and National Oceanographic and Atmospheric Administration grant NA05OAR4311134. The LES results in this study were obtained using the model of the Royal Netherlands Meteorological Institute (KNMI), using the supercomputer facilities of ECMWF in Reading, UK. The LES runs were performed by the first author when affiliated to KNMI, at that time being supported by the European Project for Cloud Systems Studies (EUROCS) as well as the Netherlands Organization for Scientific Research (NWO) under grant 750.198.06.

A. Appendix: Variance transport

The vertical variance flux is decomposed into contributions from strong updraughts and their environment,

$$\overline{w'q'q'} = a^{\mathrm{up}}\overline{w'q'q'}^{\mathrm{up}} + (1-a^{\mathrm{up}})\overline{w'q'q'}^{\mathrm{en}}, \qquad \text{(A1)}$$

where the superscript 'up' represents the average over the updraughts and 'en' represents everything else. The updraught area fraction a^{up} represents a fixed top-percentage of the tail of the PDF of vertical velocity, here taken to be 5%. The dashed line in Figure 13 shows that variance transport is dominated by the strongest updraughts, so that the environmental contribution can be neglected. The figure also shows the so-called 'top-hat' approximation for the updraught fraction, which neglects sub-ensemble internal variability. This still captures the bulk of the total transport. This suggests that

$$\frac{\partial \overline{w'q'q'}^{\mathrm{up}}}{\partial z} \approx \frac{\partial w^{\mathrm{up}}\sigma_{\mathrm{q}}^2}{\partial z} \approx w_* \frac{\partial \sigma_{\mathrm{q}}^2}{\partial z}, \qquad \text{(A2)}$$

DOI: 10.1002/qj

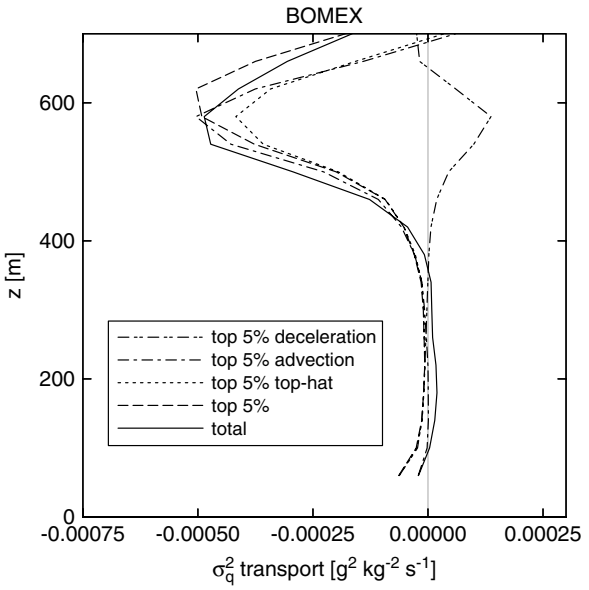

Figure 13. Various terms of the decomposition (Equations (27) and (28)) of humidity-variance transport for the BOMEX case, as sampled in LES. The strongest updraught fraction is defined as the top 5% of the PDF of vertical velocity. Included are the grid-box-mean variance transport (solid), the contribution from this top 5% (dashed), the associated top-hat approximation (dotted), and the decomposition of the latter into an advection part (dashed-dotted) and a deceleration part (dashed-double-dotted).

where the last approximation is justified by the smallness of the deceleration term $\sigma_q^2 \partial w^{up}/\partial z$: see Figure 13. Accordingly, only the term representing vertical advection of variance by the strong updraughts is retained, their vertical velocity w^{up} being assumed to scale with w_*. Then, applying the bulk-gradient approach over the top half of the mixed layer, we obtain:

$$w_* \frac{\Delta \sigma_q^2}{\Delta z} \propto \frac{\sigma_q^2\big|_h}{\tau}, \tag{A3}$$

where $\tau \sim h/w_*$ is an adjustment time-scale that can be used to describe the effect of organized transport on the variance at the top of the sub-cloud mixed layer. Here we have made use of the fact that variance in the middle of the mixed layer is typically about an order of magnitude smaller than at the top (see Figures 3 and 4).

References

Albrecht BA, Betts AK, Schubert WH, Cox SK. 1979. A model of the thermodynamic structure of the trade-wind boundary layer. Part I: Theoretical formulation and sensitivity tests. *J. Atmos. Sci.* **36**: 73–89.

Arakawa A. 2004. The cumulus parameterization problem: past, present, and future. *J. Climate* **17**: 2493–2525.

Augstein E, Riehl H, Ostapoff F, Wagner V. 1973. Mass and energy transports in an undisturbed Atlantic trade-wind flow. *Mon. Weather Rev.* **101**: 101–111.

Augstein E, Schmidt H, Wagner V. 1974. The vertical structure of the atmospheric planetary boundary layer in undisturbed trade winds over the Atlantic Ocean. *Boundary-Layer Meteorol.* **6**: 129–150.

Betts AK. 1975. Parametric interpretation of trade-wind cumulus budget studies. *J. Atmos. Sci.* **32**: 1934–1945.

Bougeault P. 1982. Cloud ensemble relations based on the gamma probability distribution for the high-order models of the planetary boundary layer. *J. Atmos. Sci.* **39**: 2691–2700.

Bretherton CS, McCaa JR, Grenier H. 2004. A new parameterization for shallow cumulus convection and its application to marine subtropical cloud-topped boundary layers. Part I: Description and 1D results. *Mon. Weather Rev.* **132**: 864–882.

Brown AR, Chlond A, Golaz C, Khairoutdinov M, Lewellen DC, Lock AP, MacVean MK, Moeng C-H, Neggers RAJ, Siebesma AP, Stevens B. 2002. Large-eddy simulation of the diurnal cycle of shallow cumulus convection over land. *Q. J. R. Meteorol. Soc.* **128**: 1075–1094.

Browning KA. 1993. The GEWEX Cloud System Study (GCSS). *Bull. Am. Meteorol. Soc.* **74**: 387–399.

Caughey SJ. 1982. Observed characteristics of the atmospheric boundary layer. In: *Atmospheric Turbulence and Air Pollution Modelling*, pp 107–158, Nieuwstadt FTM, van Dop H (eds). D. Reidel.

Cuijpers JWM, Duynkerke PG. 1993. Large-eddy simulation of trade-wind cumulus clouds. *J. Atmos. Sci.* **50**: 3894–3908.

Deardorff JW. 1974a. Three-dimensional numerical study of the height and mean structure of a heated planetary boundary layer. *Boundary-Layer Meteorol.* **7**: 81–106.

Deardorff JW. 1974b. Three-dimensional numerical study of turbulence in an entraining mixed layer. *Boundary-Layer Meteorol.* **7**: 199–226.

French JR, Vali G, Kelly RD. 1999. Evolution of small cumulus clouds in Florida: observations of pulsating growth. *Atmos. Res.* **52**: 143–165.

Grant ALM. 2001. Cloud-base fluxes in the cumulus-capped boundary layer. *Q. J. R. Meteorol. Soc.* **127**: 407–421.

Grant ALM, Brown AR. 1999. A similarity hypothesis for shallow-cumulus transports. *Q. J. R. Meteorol. Soc.* **125**: 1913–1936.

Grant ALM, Lock AP. 2004. The turbulent kinetic energy budget for shallow cumulus convection. *Q. J. R. Meteorol. Soc.* **130**: 401–422.

Holland JZ, Rasmusson EM. 1973. Measurement of atmospheric mass, energy and momentum budgets over a *500*-kilometer square of tropical ocean. *Mon. Weather Rev.* **101**: 44–55.

Joseph JH, Cahalan RF. 1990. Nearest neighbor spacing of fair weather cumulus clouds. *J. Appl. Meteorol.* **29**: 793–805.

Kaimal JC, Wyngaard JC, Haugen DA, Coté OR, Izumi Y. 1976. Turbulence structure in the convective boundary layer. *J. Atmos. Sci.* **33**: 2152–2169.

Knight CA, Miller LJ. 1998. Early radar echoes from small, warm cumulus: Bragg and hydrometeor scattering. *J. Atmos. Sci.* **55**: 2974–2992.

Laird NF, Ochs HT, Rauber TM, Miller LJ. 2000. Initial precipitation formation in warm Florida cumulus. *J. Atmos. Sci.* **57**: 3740–3751.

Lenderink G, Siebesma AP. 2000. Combining the massflux approach with a statistical cloud scheme. In: *Proceedings of the 14th AMS conference on Boundary Layers and Turbulence*, Aspen, CO, July 2000.

Lenschow DH, Wyngaard JC, Pennell WT. 1980. Mean-field and second-moment budgets in a baroclinic, convective boundary layer. *J. Atmos. Sci.* **37**: 1313–1326.

Mapes BE. 2000. Convective inhibition, subgrid-scale triggering energy, and stratiform instability in a toy tropical wave model. *J. Atmos. Sci.* **57**: 1515–1535.

Moeng C-H, Wyngaard JC. 1984. Statistics of conservative scalars in the convective boundary layer. *J. Atmos. Sci.* **41**: 3161–3169.

Neggers RAJ, Duynkerke PG, Rodts SMA. 2003. Shallow cumulus convection: A validation of large-eddy simulation against aircraft and Landsat observations. *Q. J. R. Meteorol. Soc.* **129**: 2671–2696.

Neggers RAJ, Siebesma AP, Lenderink G, Holtslag AAM. 2004. An evaluation of mass flux closures for diurnal cycles of shallow cumulus. *Mon. Weather Rev.* **132**: 2525–2538.

Neggers RAJ, Stevens B, Neelin JD. 2006. A simple equilibrium model for shallow cumulus topped mixed layers. *Theor. Comp. Fluid Dyn.* **20**: 305–322.

Nicholls S, LeMone MA. 1980. The fair weather boundary layer in GATE: the relationship of subcloud fluxes and structure to the distribution and enhancement of cumulus clouds. *J. Atmos. Sci.* **37**: 2051–2067.

Nieuwstadt FTM, Brost RA. 1986. The decay of convective turbulence. *J. Atmos. Sci.* **43**: 532–546.

Nieuwstadt FTM, Mason PJ, Moeng C-H, Schumann U. 1991. Large-eddy simulation of the convective boundary layer: A comparison of four computer codes. In: *Turbulent Shear Flows 8*, Durst F, Friedrich R, Launder BE, Schmidt FW, Schumann U, Whitelaw JH (eds). Springer: Berlin.

DOI: 10.1002/qj

Nitta T, Esbensen S. 1974. Heat and moisture budget analyses using BOMEX data. *Mon. Weather Rev.* **102**: 17–28.
Ooyama K. 1971. A theory on parameterization of cumulus convection. *J. Meteorol. Soc. Jpn* **49**: 744–756.
Siebesma AP, Cuijpers JWM. 1995. Evaluation of parametric assumptions for shallow cumulus convection. *J. Atmos. Sci.* **52**: 650–666.
Siebesma AP, Bretherton CS, Brown A, Chlond A, Cuxart J, Duynkerke PG, Jiang H, Khairoutdinov M, Lewellen D, Moeng C-H, Sanchez E, Stevens B, Stevens DE. 2003. A large eddy simulation intercomparison study of shallow cumulus convection. *J. Atmos. Sci.* **60**: 1201–1219.
Sommeria G, Deardorff JW. 1977. Subgrid-scale condensation in models of non-precipitating clouds. *J. Atmos. Sci.* **34**: 344–355.
Stevens B. 2006. Boundary layer concepts for simplified models of tropical dynamics. *Theor. Comp. Fluid Dyn.* **20**: 279–304.
Stevens B, Ackerman AS, Albrecht BA, Brown AR, Chlond A, Cuxart J, Duynkerke PG, Lewellen DC, MacVean MK, Neggers RAJ, Sanchez E, Siebsema AP, Stevens DE. 2001. Simulations of trade-wind cumuli under a strong inversion. *J. Atmos. Sci.* **58**: 1870–1891.
Stokes GM, Schwartz SE. 1994. The Atmospheric Radiation Measurement (ARM) program: programmatic background and design of the cloud and radiation test bed. *Bull. Am. Meteorol. Soc.* **75**: 1201–1222.
Stull RB. 1988. *An Introduction to Boundary Layer Meteorology*. Kluwer. 666 pp.
Tompkins A. 2002. A prognostic parameterization for the subgrid-scale variability of water vapor and clouds in large-scale models and its use to diagnose cloud cover. *J. Atmos. Sci.* **59**: 1917–1942.
Wyngaard JC, Brost RA. 1984. Top-down and bottom-up diffusion of a scalar in the convective boundary layer. *J. Atmos. Sci.* **41**: 102–112.
Wyngaard JC, Cote OR, Izumi Y. 1971. Local free convection, similarity, and the budgets of shear stress and heat flux. *J. Atmos. Sci.* **28**: 1171–1182.
Yanai M, Esbensen S, Chu J-H. 1973. Determination of bulk properties of tropical cloud clusters from large-scale heat and moisture budgets. *J. Atmos. Sci.* **30**: 611–627.
Yin B, Albrecht BA. 2000. Spatial variability of atmospheric boundary layer structure over the eastern equatorial Pacific. *J. Climate* **13**: 1574–1592.

DOI: 10.1002/qj